

# A 2D MICROGRAVITY TEST BED FOR THE VALIDATION OF SPACE ROBOT CONTROL ALGORITHMS

Submitted: 18<sup>th</sup> January 2017; accepted: 18<sup>th</sup> February 2017

*Jakub Oleś, Jan Kindracki, Tomasz Rybus, Łukasz Mężyk, Przemysław Paszkiewicz, Radosław Moczydłowski, Tomasz Barciński, Karol Seweryn, Piotr Wolański*

DOI: 10.14313/JAMRIS\_2-2017/21

## Abstract:

*The utilization of satellites equipped with robotic arms is one of the existing strategies for Active Debris Removal (ADR). Considering that the time intended for on-orbit capturing manoeuvres is strictly limited, any given space robot should possess a certain level of autonomy. This paper is about the control of on-orbit space robots and the testing of such objects in laboratory conditions. The Space Research Centre of the Polish Academy of Sciences (CBK PAN) possesses a planar air bearing microgravity simulator used for the testing of advanced control algorithms of space robots supported on air bearings. This paper presents recent upgrades to the testing facility. Firstly, the base of the space robot is now equipped with manoeuvre thrusters using compressed nitrogen and therefore allowing for position control of the entire system. Secondly, a signal from an external vision system, referencing the position and orientation of the robot's parts is used by the control system for the closed loop control.*

**Keywords:** *space debris, Active Debris Removal, Kessler syndrome, microgravity simulator, space robot, robotic arm, manipulator, control algorithm*

## 1. Introduction

### 1.1. Background

In recent years, many space agencies have become interested in controlling satellites equipped with manipulators. The aim of the DEOS [28] and e.Deorbit [2], [36] projects is the development of a technology capable observing and capturing chosen object from the Earth's orbit. Such manoeuvres could help to perform certain satellite repairs, replace broken components, refill fuel tanks or remove malfunctioning satellites from the orbit. The reason for such missions is the growing number of defunct manmade objects which remain on the Earth's orbit as space debris [20] and pose a threat to existing satellite systems, including the International Space Station (ISS) [25]. On-orbit collisions could not only cause a breakdown of active systems, but also increase the number of space debris as well as the likelihood of future collisions. Several strategies are being considered to combat this scenario, known as the Kessler syndrome [20]. Formulating safety regulations regarding space missions is one of the solutions for space debris mitigation,

which is widely used by space agencies and committees (e.g. the Inter-Agency Space Debris Coordination Committee, IADC [17], the Committee on the Peaceful Uses of Outer Space, COPUS [44], the European Space Agency, ESA [11], the National Aeronautics and Space Administration, NASA [26]).

Several ideas concerning the Active Debris Removal (ADR) are now being considered [3], [13], [40]. The capturing of large satellites and spent rocket stages [12] by a robotic arm is the most conceptually and technologically advanced solution. In the framework of the Clean Space initiative and the e.Deorbit project, several options are being investigated, e.g. the option of a robotic arm with a dedicated gripper, a huge net and an electrodynamic tether [27] which slows down any object in the Earth's magnetic field [2], [6], [14]. The idea of a satellite equipped with two manipulators and several de-orbiting kits is presented in [5]. The designing of a service spacecraft equipped with a manipulator is being handled by the Defense Advanced Research Projects Agency (DARPA) in the framework of the Robotic Servicing of Geosynchronous Satellites (RSGS) [15]. Nets [4][29] and harpoons [9] are also considered to capture objects on the orbit. Space debris deorbitation may also be accomplished by a precisely aimed laser beam, which creates a cloud of evaporated material slowing down the object and finally causing its re-entry [16], [41].

### 1.2. Testing Capabilities of Space Robots Control Systems

In this paper, an on-orbit space robot is defined as a satellite and manipulator (also called a robotic arm). The space robot subjected to tests consists of a manipulator and a base. The base represents the satellite.

The control of on-orbit space robots is a very complicated task. In order to perform the trajectory correctly, the control system has to take into account that the motion of the manipulator influences the position and orientation of the spacecraft. In subject literature, such behaviour of an object is called "free-floating" in contrast to on Earth "fixed-base" industrial robots. However, it is possible to achieve "fixed-base" conditions on orbit through active positioning and orientation maintenance of the satellite by means of manoeuvre thrusters [8].

In both cases, the control system requires a signal about the actual state of the space robot, which can be measured or estimated using a mathematical model. A manipulator can be actuated with the use of relative measurements (e.g. joint positions or end effec-

tor position with respect to target satellite position) or inertial measurements (e.g. GPS). However, inertial measurements are insufficient in the final phase of the capture manoeuvre, because high precision is required. Space robots can be tested in an analogous manner. Until now, tests of the space robot in the Space Research Centre of the Polish Academy of Sciences (CBK PAN) were performed using joint positions and a mathematical model only [31]. In extreme situations, a space robot can be controlled in an open loop, basing only on an initial state and an accurate mathematical model. However, taking into consideration that capturing with a robotic arm is a highly dynamic and risky manoeuvre, it is very important to develop a closed loop control system with signals from specialized sensors [1], [10], [18], [34], [42].

It is very difficult to perform tests of a space robot on the Earth because of the terrestrial gravity. One of the existing opportunities is to reduce the motion of a robot to a plane and use a microgravity simulator with planar air bearings. In CBK PAN tests of 2D motion are performed on a microgravity test-bed, consisting of a granite table, 2 m × 3 m wide, flat and precisely levelled, and a space robot supported on air bearings. During recent tests the completion of planned trajectories was investigated in terms of accuracy without feedback on the end effector position (but with feedback on joint positions). All trajectories, including Cartesian ones, were computed in the joint space and then sent to the robot. During the trajectory planning phase optimization methods were often used [31], [33]. In the frame of ongoing RR-SPACE project (PBS3/A3/22/2015) the test bed is being modified in order to develop a semi-autonomous space robot as a platform for the testing of various control algorithms. The modifications consist of fitting a set of manoeuvre thrusters powered by pressurized nitrogen onto the base of the space robot and using an external signal from a vision system in the control system of the robot. The thrusters, made by the Warsaw University of Technology, allow for the motion in the plane, while the vision system provides feedback on inertial positions and orientations of robotic components, therefore closing the master control loop. In this paper, the concept of such a robotic system is presented along with the testing facility and a possible exemplary test.

The paper is organized as follows: Section 2 describes 3D nonholonomic multibody system dynamics and control, as well as a point where the control input enters the system. In Section 3, modifications of the test bed are being presented. The implementation of modifications together with possible test scenarios and an exemplary simulation result are presented in Section 4. The paper is concluded in Section 5.

## 2. Space Robot Dynamics and Control

The dynamics of the satellite manipulator system is usually described with a simplifying assumption that the momentum and the angular momentum are equal to zero (e.g., [8], [22], [43]). Such assumption is not valid in the case of a space robot that uses thrusters

during the capture manoeuvre. Few authors present dynamic equations of satellite manipulator systems with a non-constant momentum and an angular momentum (e.g. [24], [39]). In this paper, we use the description of space robot dynamics based on [39].

We are considering a space robot equipped with a manipulator that has  $n$  rotational degrees of freedom (Fig. 1). Equations presented below are given in the inertial reference frame,  $CS_{ine}$ .

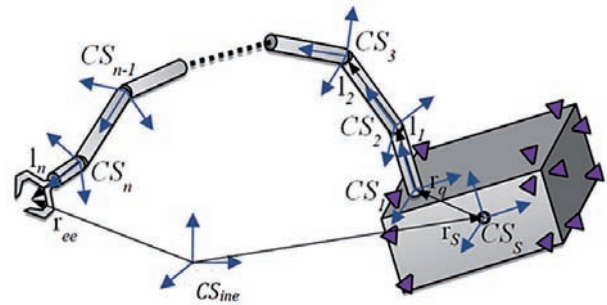


Fig. 1. A schematic view of a space robot equipped with a manipulator and thrusters

The end effector position can be expressed as:

$$\mathbf{r}_{ee} = \mathbf{r}_s + \mathbf{r}_q + \sum_{i=1}^n \mathbf{l}_i \quad (1)$$

where  $\mathbf{r}_s$  is the position of the satellite centre of mass,  $\mathbf{r}_q$  is the position of the first kinematic pair of the manipulator in respect to the satellite,  $\mathbf{l}_i$  is the position of the  $i + 1$  kinematic pair in respect to the kinematic pair  $i$  (all expressed in  $CS_{ine}$  frame). End effector velocity can be expressed as:

$$\begin{bmatrix} \mathbf{v}_{ee} \\ \boldsymbol{\omega}_{ee} \end{bmatrix} = \mathbf{J}_s \begin{bmatrix} \mathbf{v}_s \\ \boldsymbol{\omega}_s \end{bmatrix} + \mathbf{J}_M \dot{\boldsymbol{\theta}} \quad (2)$$

where  $\mathbf{v}_s$  is the linear velocity of the satellite, while  $\boldsymbol{\omega}_s$  is the angular velocity of the satellite,  $\mathbf{J}_s$  denotes the Jacobian of the satellite, while  $\mathbf{J}_M$  denotes the Jacobian of the manipulator given in the inertial reference frame,  $\dot{\boldsymbol{\theta}}$  is a  $n$ -dimensional vector that contains velocities of manipulator joints.

The satellite's Jacobian is described by:

$$\mathbf{J}_s = \begin{bmatrix} \mathbf{I} & \tilde{\mathbf{r}}_{ee,s}^T \\ \mathbf{0} & \mathbf{I} \end{bmatrix} \quad (3)$$

where  $\mathbf{r}_{ee,s} = \mathbf{r}_{ee} - \mathbf{r}_s$ ,  $\mathbf{I}$  denotes the identity matrix,  $\mathbf{0}$  is the zero matrix, the  $\tilde{\cdot}$  symbol denotes a matrix which is the equivalent of a vector cross-product.

The angular momentum of the satellite manipulator system is described by:

$$\mathbf{L} = \mathbf{L}_0 + \mathbf{r}_s \times \mathbf{P} \quad (4)$$

where  $\mathbf{L}_0$  denotes the initial angular momentum of the system.

Momentum and angular momentum are presented as:

$$\begin{bmatrix} \mathbf{P} \\ \mathbf{L}_0 + \mathbf{r}_s \times \mathbf{P} \end{bmatrix} = \mathbf{H}_2 \begin{bmatrix} \mathbf{v}_s \\ \boldsymbol{\omega}_s \end{bmatrix} + \mathbf{H}_3 \dot{\boldsymbol{\theta}} = \begin{bmatrix} \mathbf{f}_m \\ \mathbf{f}_{am} \end{bmatrix} \quad (5)$$

Matrices  $\mathbf{H}_2$  and  $\mathbf{H}_3$  (defined in [31] and [39]) are influenced not only by the state of the manipulator, but also by the state of the satellite. Functions  $\mathbf{f}_m$  and  $\mathbf{f}_{am}$  on the right hand side of equation (5) describe changes of momentum and angular momentum that are known *a priori* and depend on external forces  $\mathbf{F}_s$  and external torques  $\mathbf{H}_s$  acting on the satellite's centre of mass:  $\mathbf{f}_m = \int_{t_0}^{t_k} \mathbf{F}_s dt$  and  $\mathbf{f}_{am} = \int_{t_0}^{t_k} \mathbf{H}_s + \tilde{\mathbf{r}}_s \mathbf{F}_s dt$ , where  $t_0$  is the initial time and  $t_k$  is the final time of the maneuver. Functions  $\mathbf{f}_m$  and  $\mathbf{f}_{am}$  play a crucial role in the analysis of the space robot equipped with thrusters because these functions allow us to take into account the influence of thrusters on the satellite's dynamics. If there is an initial momentum and angular momentum of the system and no external forces/torques act on the system, then functions  $\mathbf{f}_m$  and  $\mathbf{f}_{am}$  are constant.

The non-zero right hand side of equation (5) differentiates the approach presented here from the common approach, in which zero momentum and angular momentum is assumed. Taking into account functions  $\mathbf{f}_m$  and  $\mathbf{f}_{am}$ , the end effector velocity can be described as:

$$\begin{bmatrix} \mathbf{v}_{ee} \\ \boldsymbol{\omega}_{ee} \end{bmatrix} = \mathbf{J}_s \mathbf{H}_2^{-1} \begin{bmatrix} \mathbf{f}_m \\ \mathbf{f}_{am} \end{bmatrix} + (\mathbf{J}_M - \mathbf{J}_s \mathbf{H}_2^{-1} \mathbf{H}_3) \dot{\boldsymbol{\theta}} \quad (6)$$

The following kinematic relation between the end effector velocity and velocities of manipulator joints can be obtained using:

$$\dot{\boldsymbol{\theta}} = (\mathbf{J}_M - \mathbf{J}_s \mathbf{H}_2^{-1} \mathbf{H}_3)^{-1} \left( \begin{bmatrix} \mathbf{v}_{ee} \\ \boldsymbol{\omega}_{ee} \end{bmatrix} - \mathbf{J}_s \mathbf{H}_2^{-1} \begin{bmatrix} \mathbf{f}_m \\ \mathbf{f}_{am} \end{bmatrix} \right) \quad (7)$$

while the linear and angular velocity of the manipulator-equipped satellite is described by:

$$\begin{bmatrix} \mathbf{v}_s \\ \boldsymbol{\omega}_s \end{bmatrix} = \mathbf{H}_2^{-1} \left( \begin{bmatrix} \mathbf{f}_m \\ \mathbf{f}_{am} \end{bmatrix} - \mathbf{H}_3 \dot{\boldsymbol{\theta}} \right) \quad (8)$$

Equation (7) can be used when the manipulator has 6 DoF. If a redundant manipulator is used, then  $\mathbf{J}_M$  is a non-square matrix and it is necessary to use pseudoinverse in equation (7). A transformation matrix between the inertial reference frame and the body-fixed coordinate system is determined through kinematic equations by the angular velocity of the servicing satellite ( $\boldsymbol{\omega}_s$ ). Equations (7) and (8) are used by the trajectory planning algorithm (in cases where actions of thrusters are known at the trajectory planning stage, before the execution of the manoeuvre). We use Lagrangian formalism to derive dynamics equations. To describe the state of the system, we chose the following generalized coordinates [19]:

$$\mathbf{q} = [\mathbf{r}_s^T \quad \boldsymbol{\theta}_s^T \quad \boldsymbol{\theta}^T]^T \quad (9)$$

where  $\boldsymbol{\theta}_s$  denotes the orientation of the satellite (given by its three Euler angles). The potential energy

is not taken into account as in the short timeframe of the capture manoeuvre, it remains almost constant. The Lagrange equation has the following form:

$$\frac{d}{dt} \left( \frac{\partial \mathbf{T}}{\partial \dot{\mathbf{q}}} \right) - \left( \frac{\partial \mathbf{T}}{\partial \mathbf{q}} \right) = \mathbf{Q} \quad (10)$$

where  $\mathbf{T}$  is the kinetic energy of the system, while  $\mathbf{Q} = [\mathbf{F}_s^T \mathbf{H}_s^T \mathbf{u}^T]^T$  is the vector of generalized forces, in which  $\mathbf{u}$  denotes the vector of control torques applied in the manipulator joints.

Modified version of Equation (10) is used to derive the general equations of motion for space robot. These equations can be used to compute control torques  $\mathbf{u}(t)$  required to perform planned motion of the end effector:

$$\mathbf{Q} = \mathbf{M}(\mathbf{q})\ddot{\mathbf{q}} + \mathbf{C}(\dot{\mathbf{q}}, \mathbf{q})\dot{\mathbf{q}} \quad (11)$$

where  $\mathbf{M}$  denotes the mass-matrix, while  $\mathbf{C}$  denotes the Coriolis matrix (details can be found in [31] and [39]).

In the equation (11), potential forces are not taken into account, because the satellite is in the state of free fall.

### 3. Modifications of Testing System

Former testing system, described in [30], consisted of the base and two-link manipulators, both supported by air bearings for frictionless motion. It allowed for the realisation of pre-planned trajectories both in Cartesian and configuration space with no feedback on the position of the end effector. In order to plan trajectories in Cartesian space, algorithms based on dynamic Jacobian were used to take into account the "free-floating" state of the system and the high ratio of the manipulator mass versus the mass of the base. Results of the tests were then compared with corresponding simulations.

There are two modifications of the testing system described in this paper. The first one is related to the space robot control system, specifically to the access of the control system to the inertial position and orientation. The second one affects the satellite body by adding a set of cold gas thrusters which allow its motion in the plane.

In the general approach, the control torques in manipulator joints are a composition of feed forward torques  $\mathbf{u}_{ref}$ , calculated in the trajectory planning phase and correction torques  $\mathbf{u}_{contr}$ , computed by the control system during motion in real time (12). The measurement of position and velocity of the end effector ( $\mathbf{r}_{ee}, \mathbf{v}_{ee}$ ), which is necessary for the computation of  $\mathbf{u}_{contr}$ , can be obtained from the vision system (described in detail in 3.1). Thus,

$$\mathbf{u} = \mathbf{u}_{ref} + \mathbf{u}_{contr}(\mathbf{e}_p, \mathbf{e}_v) \quad (12)$$

where the position and velocity error are defined as follows:

$$\mathbf{e}_p = \mathbf{r}_{ee} - (\mathbf{r}_{ee})_{ref} \quad (13)$$

$$\mathbf{e}_v = \mathbf{v}_{ee} - (\mathbf{v}_{ee})_{ref} \quad (14)$$

The feedback on the position and velocity of the end effector is crucial during capturing manoeuvres. Manoeuvre thrusters, which are added to the base as the second modification (described in detail in 3.2), are responsible for the generation of forces and torques ( $\mathbf{F}_s, \mathbf{H}_s$ ) acting on the base centre of mass. Forces  $\mathbf{F}_s$  and torques  $\mathbf{H}_s$  are then used in both the dynamic analysis and the control system.

In the 2D system, the equation describing the control problem concerning the base can be stated as follows:

$$\begin{bmatrix} F_x \\ F_y \\ \tau_z \end{bmatrix} = \mathbf{A}^{3 \times 8} \mathbf{f} \quad (15)$$

where forces acting on the eight cold gas thrusters (the outputs) are:

$$\mathbf{f} := [f_1 \dots f_8]^T \quad (16)$$

and:

$F_x, F_y$  – resultant forces, respectively in  $x$  and  $y$  direction in the base reference frame (components of  $\mathbf{F}_s$  in 2D case),

$\tau_z$  – a torque with respect to the  $z$  direction (component of  $\mathbf{H}_s$  in 2D case),

$\mathbf{A}^{3 \times 8}$  – a matrix transposing forces at 8 cold gas thrusters to resultant force and torque.

The control of the base is formulated as follows:

$$\mathbf{f} = \mathbf{A}^\# \begin{bmatrix} F_x \\ F_y \\ \tau_z \end{bmatrix} \quad (17)$$

where  $\mathbf{A}^\#$  is the Moore-Penrose pseudoinverse of the matrix  $\mathbf{A}^{3 \times 8}$ .

The use of pseudoinverse allows for the finding of a solution of a minimum Euclidean norm among all possible solutions. It therefore minimizes the flow rate during trajectory performance in the described system. This operation distributes force equally to the specific pairs of thrusters. As a result, the pairs with the same force value and opposite signs are obtained. Therefore, negative values have to be rejected and the others, doubled in order to achieve the same effect on the base.

In current 2D simulations, matrix  $\mathbf{A}^\#$  takes the following form:

$$\mathbf{A}^\# = \begin{bmatrix} -a & -c & c & a & g & -c & c & -g \\ b & -d & -h & -b & b & h & d & -b \\ e & -e & e & -e & e & -e & e & -e \end{bmatrix}^T \quad (18)$$

where:  $a = 0.2492, b = 2.2e^{-4}, c = -7.99e^{-4}, d = 0.25022, e = 0.625, g = 0.2508, h = 0.24987$ .

In the current approach, specific control schemes are used: a control scheme based on the dynamic Jacobian inverse [35] for the manipulator and PD controller for the base. Each of them is based on the feedback on the position and orientation of the base and position of the end effector provided by the vision system. Simulations have shown that depending on the type of the base trajectory (line, arc, rotation, line + rotation, etc.) different correcting gains in the PD controller have to be used to ensure good trajectory realization accuracy.

### 3.1. Vision System

The feedback mentioned in Eq. (13) depends on acquisition time. It is realized by an external vision system delivered by OptiNav, which consists of 3 industrial cameras of 5 MPx resolution and 100 Hz frequency, as well as a PC with dedicated software for visual marker recognition. The results are transferred by wireless communication to the control system on the space robot computer.

The space robot on the test bed is extremely sensitive to any force coming from its surroundings. Therefore, the wireless connection for data transfer is used to avoid the influence of cables on the platform motion [37]. In order to correctly use the data obtained from the vision system, we have to ensure that the time instant of image acquisition ( $t_{aq}$ ) is specified in the space robot computer time frame. The necessity of using wireless communication and fulfilling the above-mentioned requirements creates a problem, which is solved in two steps. First of all, the space robot sends a signal to the cameras triggering device, together with a unique time tag, which is then being added to the results of the processing of the acquired image. This ensures that the computer in the space robot can locate the time instant ( $t_{aq}$ ) from which the received data from the vision system comes. Secondly,

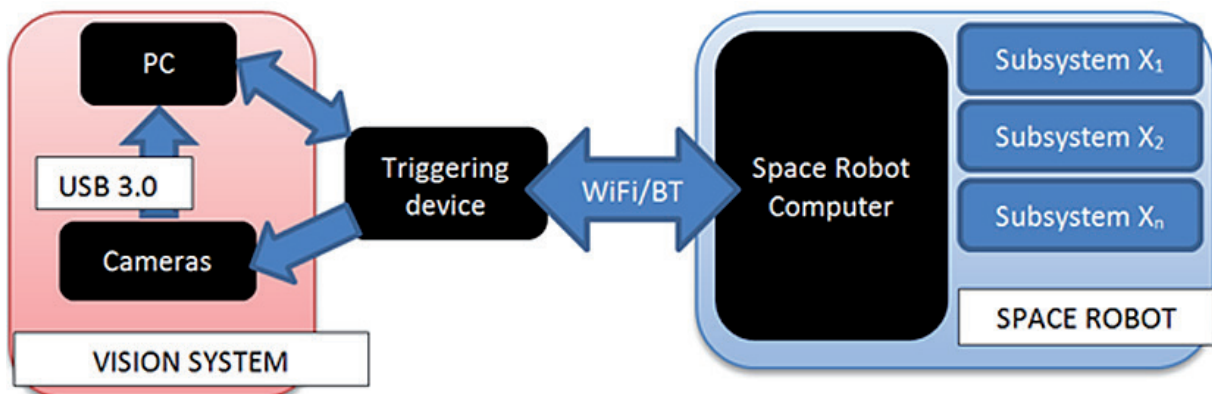


Fig. 2. Signal transfer in the system

a synchronization of processors on the space robot and the triggering device is performed by a special Bluetooth protocol with an accuracy of 3 ms. The total delay between sending the triggering signal and receiving the data, which is estimated at 80–100 ms, does not impair the quality of control. This is due to the fact that the data from the vision system is used as a correction of IMU readouts in the Kalman filter. The scheme of the system is shown in Fig. 2.

The described system represents a real on orbit case in which the servicing robot approaches the target using GPS navigation in inertial reference frame. During the process of capturing, which is the relative navigation phase, cameras and laser proximity sensors are used. Star trackers could also be used to correct readings from IMU. The test facility can simulate both cases in the presence of two or more objects on the test bed. By default, the vision system works in inertial reference frame but it is possible to compute relative distances and orientations to use them in non-inertial frame. The formulation of the control function  $\mathbf{u}_{contr}$  is not a part of this paper.

### 3.2. Robotic Platform

In the framework of the RR-SPACE project, an existing base of a space robot was used. The base was enhanced by mounting 8 cold gas thrusters with a separate gas canister with pressurized nitrogen (Fig. 3). The gasses used in the experiment were

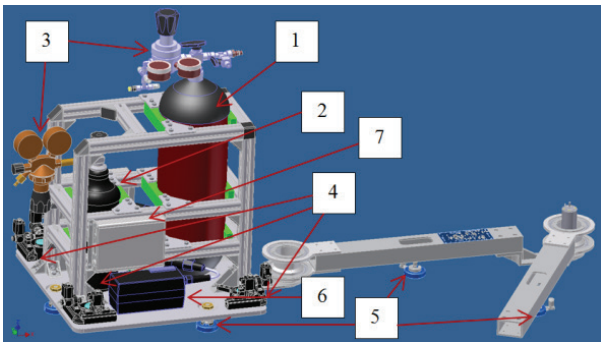


**Fig. 3.** The space robot. 1 – a gas canister with compressed nitrogen for cold gas thrusters, 2 – a gas canister with compressed air for air bearings, 3 – pressure regulators, 4 – cold gas thrusters, 5 – air bearings, 6 – battery, 7 – electronic box

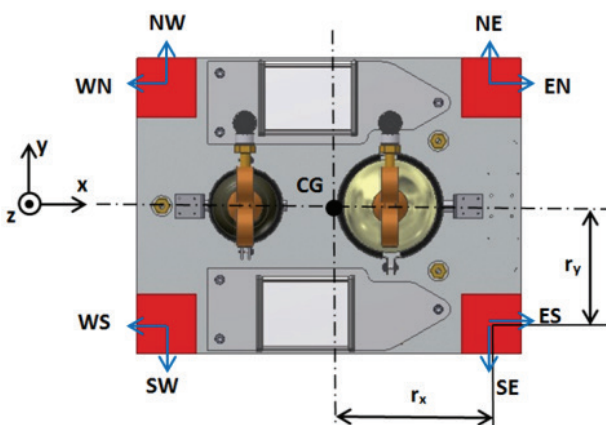


**Fig. 4.** Locations of cold gas thrusters on the base of the space robot,  $r_x = r_y = 200\text{mm}$

chosen for their safety for the space robot and technical operators. The expelled nitrogen does not affect any physical components of the space robot.

Cold gas thrusters were mounted on the corners of the base, pointing in perpendicular directions (Fig. 4). Such a location allows for complete position and orientation control.

Mass and geometry parameters were chosen as guided by scaling laws. Scaling is usually performed when it is difficult to test the object in 1:1 scale due to both manufacturing costs and testing facility capabilities. Instead, dimensions of the testing mockup can be minimized with the use of scaling laws. Moreover, the obtained upon re-scaling results can be used for the analysis of the full scale object. The equation of scaling law is presented in (19).

$$P_s = k^w P \quad (19)$$

where:  $P_s$  – value after scaling,  $k$  – scaling coefficient,  $w$  – scaling exponent,  $P$  – value before scaling.

Several exemplary scaling exponents for specific physical properties are shown in Tab. 1.

**Tab. 1.** Physical properties with scaling exponents [7]

Physical property	Scaling exponent	Physical property	Scaling exponent
Distance	1	Inertia	5
Time	1	Velocity	0
Frequency	-1	Acceleration	-1
Force	2	Energy	3
Mass	3	Power	2

In Tab. 2, some assumed parameters of a real space mission are presented together with parameters of a scaled test platform in CBK PAN.

**Tab. 2.** The scaling of the space robot

Parameter	Real space robot (3D)	Space robot in CBK PAN (2D)
Total mass $m_c$ [kg]	570.00	66.16
Mass of the base $m_b$ [kg]	518.18	60.15
Mass of the manipulator $m_m$ [kg]	51.82	6.01
Manipulator length $l_m$ [m]	2.50	1.22
Base inertia $I_b$ [kg*m <sup>2</sup> ]	-	2.199
Ratio $m_m/m_b$ [-]	0.10	0.10
Ratio $m_m/m_c$ [-]	0.09	0.09
Scaling exponent $k$	-	0.4878
$1/k$ [-]	-	2.05

The influence of the degree of filling of the gas canister with compressed air for the air-bearings and the gas canister with compressed nitrogen for cold gas thrusters was also analyzed. Several cases were distinguished: (i) both canisters are full, (ii) both canisters are empty, (iii) the canister for air bearings is

full and the canister for thrusters is empty, (iv) the canister for air bearings is empty and the canister for thrusters is full. The parameters of the base for each of the distinguished cases were evaluated using the CAD model and shown in Tab. 3.

**Tab. 3. Parameters of the base per analyzed case**

Case		(i)	(ii)	(iii)	(iv)
<b>Mass [kg]</b>		60.017	59.227	59.617	59.627
<b>CoG position [mm]</b>	x	0.354	0.333	-0.415	1.102
	y	-1.279	-1.297	-1.288	-1.288
	z	105.361	104.098	104.32	105.147
<b>Inertia I<sub>zz</sub> [kg*m<sup>2</sup>]</b>		2.384	2.372	2.378	2.378

Performed analysis showed that the influence of the level of usage of the gasses on the parameters of the base is negligible. The mass of the base changes by 1.3% and the inertia, by 0.5%. The minimal influence should be seen only during experiments conducted in open-loop mode. The influence can be neglected in the closed loop mode.

According to tests of the cold gas engine specially designed for experiments, described in details in [21], several parameters can be identified. The nominal thrust of the cold gas engine is 0.846 N, the nominal chamber pressure is 10 bar and the mass flow rate is 1.575 g/s. Some dynamic parameters were also identified. The opening time for the 13.7 W electromagnetic coil is 3.15 ms and the delay in the opening time is 5.5 ms. Therefore, the minimal time of

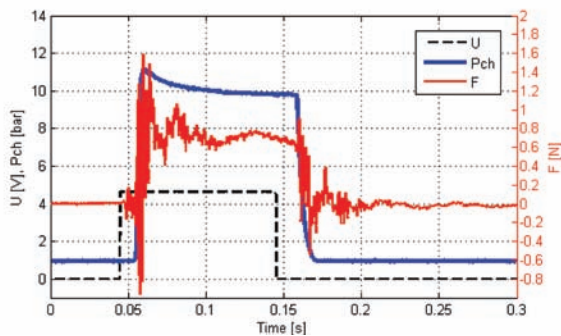


**Fig. 5. Trigger U, thrust force and chamber pressure during a 100 ms' thrust**

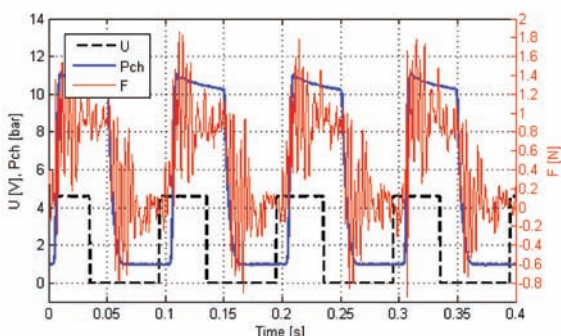


**Fig. 6. Trigger U, thrust force and chamber pressure operating with 10 Hz frequency and a 40 ms' thrust**

thrust is 15 ms and the maximal frequency (in PWM mode) is 35 Hz. Exemplary characteristics with thrust force and chamber pressure are shown in Fig. 5. and Fig. 6.

**4. Results**

**4.1. Test-bed Implementation**

The modifications described in Section 3 were implemented in the test bed system shown in Fig. 7. It consists of a granite table, which is 2 m × 3 m wide, flat and precisely levelled, a space robot mockup and a vision system with dedicated software on an external PC. The space robot can move freely on the surface of the table using air bearings.



**Fig. 7. The test-bed. 1 – the air bearing table, 2 – the space robot, 3 – the illumination system, 4 – vision system cameras**

**4.2. Exemplary Test Scenario**

There are several possible aspects that can be investigated in the facility. For example, the influence of a compliant joint with magnetic gear on the accuracy of trajectory realization can be tested. A new robust control system can be developed for this case. The aspect of position and orientation control of the base with 8 manoeuvre thrusters along with trajectory realization may become an area for further research. The most complicated case is when both the base and the end effector have their separate trajectories (Fig. 8). Two phenomena manifest here: one is that the thrusters introduce a non-constant linear and angular momentum into the system and

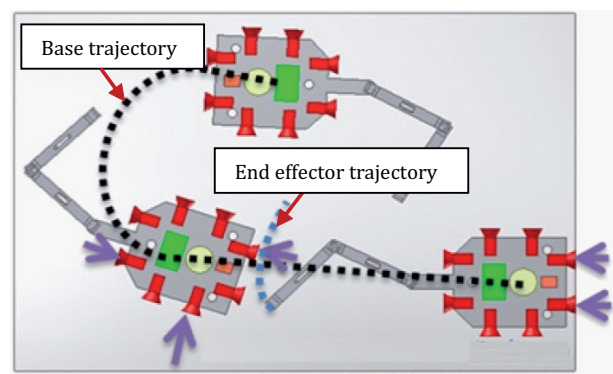


**Fig. 8. A possible test with trajectories for the base and for the end effector (red – cold gas thrusters, green – one of the components, arrows – thrust forces)**

the second one is that the motion of the manipulator causes force reactions to act on the base. The correct undertaking of the test is possible due to feedback from the vision system.

This case represents the real on orbit case in which a satellite has an active Attitude and Orbit Control System (AOCS), but the system does not maintain the satellite's position and orientation. The main goal of this activity is to develop a robust testing research platform for various control algorithms of the space robot. The secondary goal is to verify the accuracy of the trajectory performance of the manipulator and to test several control algorithms.

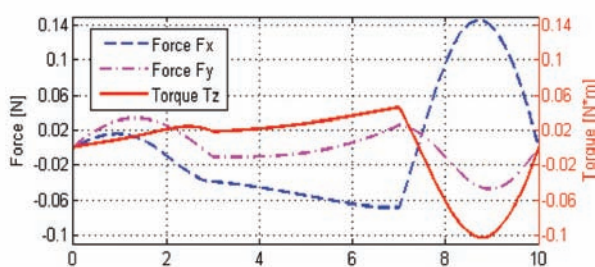
The nominal mode of operation of the space robot comprises the realization of two separate trajectories: for the base and the robotic arm at the same time. However, several other modes can be distinguished:

- the motion of the base versus the given position and orientation (inertial space),
- the realization of the trajectory for the base only,
- the motion of the robotic arm versus the given position in configuration space,
- the realization of the trajectory for the robotic arm in configuration space,
- the motion of the robotic arm to the given point for the end effector (inertial space),
- the realization of the trajectory for the end effector only, given in inertial space.

The control system on the space robot computer consists of several function blocks: Guidance (which receives data from sensors), Navigation (filters) and the Control function block. Therefore, the space robot is prepared to apply different control algorithms by changing control schemes in the Control function block.

### 4.3. Simulation Result

In the simulation prepared in the MATLAB®/Simulink environment, the manipulator performed the linear trajectory in an inertial space and the cold gas thrusters were used to maintain the position and orientation of the base. This case represents an on orbit situation in which the AOCS controls the state of the satellite and actively counteracts the loads resulting from the manipulator's movement. Such a case is usually described as "fixed-base" in contrast to the case when the AOCS is turned off completely (the case of "free-floating"). The open-loop control scheme based on the dynamic Jacobian inverse [35] was used for robotic arm movement and the open-loop algorithm was used for base stabilization.



Tab. 4. Simulation parameters

Parameter	Value
Inertia of the base [ $\text{kg} \cdot \text{m}^2$ ]	2.199
Base and manipulator mass [ $m_b; m_m$ ] [kg]	[60.15; 6]
Time of simulation [s]	10
Time of acceleration and deceleration [ $t_p; t_n$ ] [s]	[3, 3]
Initial end effector position [ $x; y$ ] [m]	[0.8; 0.7]
Initial end effector velocity [ $v_x; v_y$ ] [m/s]	[0, 0]
Final end effector position [ $x; y$ ] [m]	[0.8; 0.1]
Final end effector velocity [ $v_x; v_y$ ] [m/s]	[0, 0]

The parameters used in the simulation are shown in Tab. 4. The motion of the end effector was planned as to have acceleration part of time  $t_p$  and deceleration part of time  $t_n$ .

Fig. 9 (on the left hand side) shows reactions acting on the base centre of mass, resulting from the manipulator's motion. The task of the stabilization of the base's position and orientation by counteracting these reactions was performed by a set of 8 cold gas thrusters. The force on each thruster was calculated using equation (17) and shown in Fig. 10. In the presented configuration, the maximal value of force on a single thruster is 0.2 N. The thrust force on a single thruster is 0.86 N. The conclusion is that the stabilization of the base in given conditions should be viable. What is worth noting about thrusters is that they provide an impulse thrust and it is therefore impossible to achieve intermediate values of thrust force. This issue can be resolved by using either short period thrusts or a kind of PWM mode. To check the influence of the impulse operation mode of thrusters on the accuracy of base stabilization, two simulations were performed:

- the forces shown in Fig. 10 were applied to the base directly without any change. It means that the thrusters did not work in the impulse mode,
- the forces shown in Fig. 10 were calculated to impulse in the PWM mode with a frequency of 5 Hz and a duty cycle depending on the force value.

As a result, a total base position and orientation error was obtained (Fig. 9). In the PWM mode, the base orientation error is bigger, with a maximal value of 0.12 deg, compared to 0.08 deg. However, the base position error in the PWM mode is lower, with a maximal value of  $1.35 \cdot 10^{-4}$  m compared to  $1.55 \cdot 10^{-4}$  m.

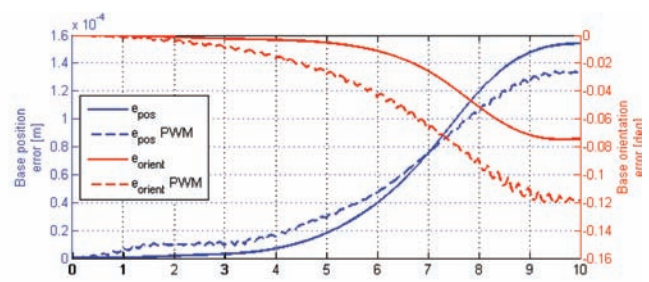
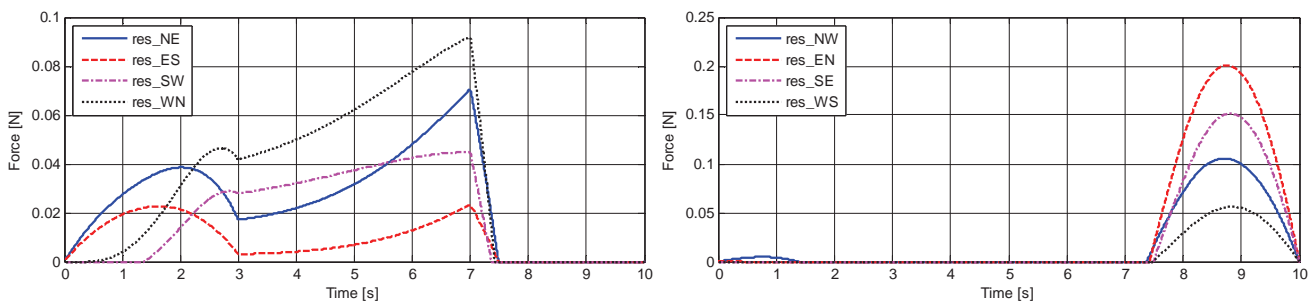


Fig. 9. Left: Forces and torque acting on the base center of gravity. Right: Position and orientation errors during the realization of the base trajectory



**Fig. 10. Forces on cold gas engines necessary for the stabilization of the base in the Cartesian trajectory realization**

The simulation showed that the thruster's impulse operation mode did not affect the accuracy of the base stabilization. Any possible negative effects of impulse mode during trajectory realization should be, however, negligible in experiments performed in closed loop mode with feedback from the vision system.

## 5. Summary

The context of this paper is the problem of space debris mitigation, as well as select strategies to limit its amount on the Low Earth Orbit (LEO). In this study, the investigation was limited to the phenomenon of control of a space robot equipped with a manipulator arm. In the paper, the recent modifications of the test bed in CBK PAN referencing a microgravity simulation in a plane were presented. The test bed is capable of testing various control systems and performing complex manoeuvres, simulating the capturing of space debris. The vision system provides a position and orientation signal for the closed loop mode, which enables the testing of more complicated cases. Future research will focus on the relative navigation during the final phase of the rendezvous manoeuvre. Tests may be performed with a virtual or real target. Tests related to the formation flight are also being foreseen. The isolation of the space robot from external world is a huge advantage concerning contact tests, e.g. those involving grippers and landers.

## ACKNOWLEDGEMENTS

This paper was supported by the National Centre for Research and Development, project no. PBS3/A3/22/2015.

## AUTHORS

**Jakub Oleś\*** – Space Research Centre of the Polish Academy of Sciences (CBK PAN), Bartycka 18a str., 00-716 Warsaw, Poland, joles@cbk.waw.pl.

**Jan Kindracki** – Institute of Heat Engineering, Warsaw University of Technology, Nowowiejska 21/25 str., 00-665 Warsaw, Poland.

**Tomasz Rybus** – Space Research Centre of the Polish Academy of Sciences (CBK PAN), Bartycka 18a str., 00-716 Warsaw, Poland.

**Łukasz Mężyk** – Institute of Heat Engineering, Warsaw University of Technology, Nowowiejska 21/25 str., 00-665 Warsaw, Poland.

**Przemysław Paszkiewicz** – Institute of Heat Engineering, Warsaw University of Technology, Nowowiejska 21/25 str., 00-665 Warsaw, Poland

**Radosław Moczydłowski** – Space Research Centre of the Polish Academy of Sciences (CBK PAN), Bartycka 18a str., 00-716 Warsaw, Poland.

**Tomasz Barciński** – Space Research Centre of the Polish Academy of Sciences (CBK PAN), Bartycka 18a str., 00-716 Warsaw, Poland.

**Karol Seweryn** – Space Research Centre of the Polish Academy of Sciences (CBK PAN), Bartycka 18a str., 00-716 Warsaw, Poland.

**Piotr Wolański** – Institute of Heat Engineering, Warsaw University of Technology, Nowowiejska 21/25 str., 00-665 Warsaw, Poland.

\*Corresponding author

## REFERENCES

- [1] Barciński T, Lisowski J, Rybus T, Seweryn K, "Controlled Zero Dynamics Feedback Linearization with Application to Free-Floating Redundant Orbital Manipulator". In: *2013 IEEE American Control Conference*, Washington DC, USA, 2013, 1834–1839. DOI: 10.1109/ACC.2013.6580102.
- [2] Biesbroeck R., "The e.Deorbit Study in the Concurrent Design Facility", The CleanSpace: Workshop, Darmstadt, September 2012.
- [3] Bonnal C., Ruault J., Desjean M., "Active Debris Removal: Recent Progress and Current Trends", *Acta Astronautica* 85, 2013, 51–60. DOI: 10.1016/j.actaastro.2012.11.009.
- [4] Botta E., Sharf I., Misra A., Teichmann M., "On the Simulation of Tether Nets for Space Debris Capture with Vortex Dynamics", *Acta Astronautica*, 123, 2016, 91–102. DOI: 10.1016/j.actaastro.2016.02.012.
- [5] Castronuovo M., "Active Space Debris Removal – A Preliminary Mission Analysis and Design", *Acta Astronautica*, 69, 2011, 848–859. DOI: 10.1016/j.actaastro.2011.04.017.

- [6] Clean Space, “e.Deorbit Implementation Plan”, ESA-TEC-SC-TN-2015-007, 2015.
- [7] Dexler K., *Nanosystems: Molecular Machinery, Manufacturing, and Computation*, Wiley, 1998.
- [8] Dubowsky S., Papadopoulos E., “The Kinematics, Dynamics and Control of Free-Flying and Free-Floating Space Robotic Systems”, *IEEE Transaction on Robotics and Automation*, vol. 9, no. 5, 1993, 531–543. DOI: 10.1109/70.258046.
- [9] Dudziak R., Tuttle S., Barraclough S., “Harpoon Technology for the Active Removal of Space Debris”, *Advances in Space Research*, 56, 2015, 509–527. DOI: 10.1016/j.asr.2015.04.012.
- [10] Duleba I., *Algorithms of Motion Planning for Non-holonomic Robots*, Oficyna Wydawnicza Politechniki Wrocławskiej, Wrocław 1998.
- [11] European Space Agency, International Academy of Astronautics, “Position Paper on Space Debris Mitigation; Implementing Zero Debris Zones”, Noordwijk, 2006.
- [12] Felicetti L. et al., “Design of Robotic Manipulators for Orbit Removal of Spent Launchers’ Stages”, *Acta Astronautica*, 119, 2016, 118–130. DOI: 10.1016/j.actaastro.2015.11.012.
- [13] Forshaw J. et al., “RemoveDEBRIS: An In Orbit Active Debris Removal Demonstration Mission”, *Acta Astronautica*, 2016, 448–463. DOI: 10.1016/j.actaastro.2016.06.018.
- [14] Hausmann G. et al., “e.Deorbit Mission: OHB Removal Concepts”. In: *ASTRA 13<sup>th</sup> Symposium on Space Technologies in Robotics and Automation*, The Netherlands, 2015.
- [15] Henshaw C., “The DARPA Phoenix Spacecraft Servicing Program: Overview and Plans for Risk Reduction. International Symposium on Artificial Intelligence”, *Robotics and Automation in Space (i-SAIRAS)*, Montreal, 2014.
- [16] Hou L., Cai Y., Liu J., Hou Ch., “Variable Fidelity Robust Optimization of Pulsed Laser Orbital Debris Removal Under Epistemic Uncertainty”, *Advances in Space Research*, 57, 2016, 1698–1714. DOI: 10.1016/j.asr.2015.12.003
- [17] Inter-Agency Space Debris Coordination Committee, “IADC Space Debris Mitigation Guidelines”, Rev.1, September 2007.
- [18] Jarzębowska E., Pietrak K., “Constrained Mechanical Systems Modeling and Control: A Free-Floating Space Manipulator Case as a Multi-Constrained System”, *Robotics and Autonomous Systems*, 62, 2014, 1353–1360. DOI: 10.1016/j.robot.2014.04.004.
- [19] Junkins J. L., Schaub H., “An Instantaneous Eigenstructure Quasivelocety Formulation for Nonlinear Multibody Dynamics”, *Journal of the Astronautical Sciences*, vol. 45, no. 3, 1997, 279–295.
- [20] Kessler D. J. et al., “The Kessler Syndrome: Implications to Future Space Operations”, *Advances in the Astronautical Sciences*, 137, no. 8, 2010.
- [21] Kindracki J., Tur K., Paszkiewicz P., Mężyk Ł., Boruc Ł., Wolański P., “Experimental Research on Low-cost Cold Gas Propulsion for a Space Robot Platform”, *Aerospace Science and Technology*, 62, 2017, 148–157. DOI: 10.1016/j.ast.2016.12.001.
- [22] Lindberg R.E., Longman R.W., Zedd M.F., “Kinematic and Dynamic Properties of an Elbow Manipulator Mounted on a Satellite”. In: *Space Robotics: Dynamics and Control*, Ed.: Y. Xu and T. Kanade, Springer, USA, 1993. DOI: 10.1007/978-1-4615-3588-1\_1.
- [23] Mężyk Ł., Paszkiewicz P., Kindracki J., Boruc Ł., “Experimental Research on Hydrogen Peroxide Micro Thruster for Satellite Application”. In: *Proceedings from the IX International Scientific Conference „Development Trends in Space Propulsion Systems”*, Warsaw, Poland, 2015, 148–157, 10.1016/j.ast.2016.12.001.
- [24] Nanos K., Papadopoulos E., “On the Use of Free-Floating Space Robots in the Presence of Angular Momentum”, *Intelligent Service Robotics*, vol. 4, no. 1, DOI: 2011, 3–15. 10.1109/AIM.2010.5695904.
- [25] *NASA Orbital Debris Quarterly News*, “Increase in ISS Debris Avoidance Manoeuvres”, Vol. 16, issue 2, April 2012.
- [26] NASA Procedural Requirements for Limiting Orbital Debris, NPR 8715\_006A, 2009.
- [27] Nishida S. et al., “Space Debris’ Removal System Using a Small Satellite”, *Acta Astronautica* 65, 95-102, 2009, 95–102. 10.1016/j.actaastro.2009.01.041
- [28] Reintsema D. et al., “DEOS – the German Robotics Approach to Secure and De-Orbit. Malfunctioned Satellites from Low Earth Orbit”, *International Symposium on Artificial Intelligence, Robotics and Automation I Space (i-SAIRAS)*, 2010.
- [29] Retat I. et al., “Net Capture System; a Potential Orbital Space Debris Removal System”, 2<sup>nd</sup> European Workshop on Active Debris Removal, Paris, June 2012.
- [30] Rybus T. et al., “New Planar Air-bearing Microgravity Simulator for Verification of Space Robotics Numerical Simulations and Control Algorithms”, 12<sup>th</sup> Symposium on Advanced Space Technologies in Robotics and Automation (ASTRA 2013), ESTEC, Noordwijk, The Netherlands, 2013.
- [31] Rybus T., Seweryn K., “Manipulator Trajectories During Orbital Servicing Mission: Numerical Simulations and Experiments on Microgravity Simulator”, 6<sup>th</sup> European Conference for Aeronautics and Space Sciences (EUCASS 2015), Kraków, Polska, 2015, 377–394.
- [32] Rybus T., Seweryn K., “Planar Air-Bearing Microgravity Simulators: Review of Applications, Existing Solutions and Design Parameters”, *Acta Astronautica* 120, 2016, 239-259. 10.1016/j.actaastro.2015.12.018
- [33] Rybus T., Seweryn K., Sasiadek J., “Application of Trajectory Optimization Method for a Space Manipulator with Four Degrees of Freedom”, 11<sup>th</sup> AAIA Conference, 2016, 92–101.
- [34] Rybus T., Seweryn K., Sasiadek J., “Control System for Free-Floating Space Manipulator Based

- on Nonlinear Model Predictive Control (NMPC)", *Journal of Intelligent and Robotic Systems*, 2016, 491-509. DOI: 10.1007/s10846-016-0396-2.
- [35] Rybus, T., Barcinski, T., Lisowski, J., Seweryn, K. "Analyses of a Free-Floating Manipulator Control Scheme Based on the Fixed-Base Jacobian with Spacecraft Velocity Feedback" Sasiadek, J.Z. (ed.) *Aerospace Robotics II, GeoPlanet: Earth and Planetary Sciences*, Springer-Verlag, 2015, 59-69.
- [36] Scheper M., "e.Deorbit Phase B1", *Clean Space Industrial Days*, ESTEC, Noordwijk, The Netherlands, 2016.
- [37] Seweryn K. *et al.*, "Design and Development of Two Manipulators as a Key Element of a Space Robot Testing Facility", *Archive of Mechanical Engineering*, vol. LXII, no. 3, 2015, 377-394. DOI: 10.1515/meceng-2015-0022.
- [38] Seweryn K., „Dynamika manewru zbliżania satelitów i ich połączenia za pomocą manipulatora o więzach nieholonomicznych” (The dynamics of maneuvering of satellites and their connection with a manipulator with non-holistic constraints), PhD thesis, Warsaw University of Technology, 2008. In Polish.
- [39] Seweryn K., Banaszekiewicz M., "Optimization of the Trajectory of a General Free-Flying Manipulator During the Rendezvous Manoeuvre", *AIAA Guidance, Navigation, and Control Conference and Exhibit*, Honolulu, Hawaii, USA, 2008. DOI: 10.2514/6.2008-7273.
- [40] Shan M., Guo J., Gill E., "Review and Comparison of Active Space Debris Capturing and Removal Methods", *Progress in Aerospace Sciences*, 80, 2016, 18-32. DOI: 10.1016/j.paerosci.2015.11.001.
- [41] Soulard R., Quinn M., Tajima T., Mourou G., "ICAN: A Novel Laser Architecture for Space Debris Removal", *Acta Astronautica*, 105, 2014, 192-200. DOI: 10.1016/j.actaastro.2014.09.004.
- [42] Ulrich S., Sasiadek J., Barkana I., "Modeling and Direct Adaptive Control of a Flexible-Joint Manipulator", *J. Guid. Control. Dynam.*, vol. 35, no. 1, 2012, 25-39. DOI: 10.2514/1.54083.
- [43] Umetani Y., Yoshida K., "Resolved Motion Rate Control of Space Manipulators with Generalized Jacobian Matrix", *IEEE Transactions on Robotics and Automation*, vol. 5, no. 3, 1989, 303-314. DOI: 10.1007/978-1-4615-3588-1\_7.
- [44] United Nations Office for Outer Space Affairs, "Space Debris Mitigation Guidelines of the Committee on the Peaceful Uses of Outer Space", Vienna 2010.